Electrochemical Tip-Enhanced Raman Spectroscopy for the Elucidation of Complex Electrochemical Reactions

Alice Fiocco, Aja Pavlic, Frédéric Kanoufi, Emmanuel Maisonhaute, Jean-Marc Noël, Ivan Lucas

Electrochemical Tip-Enhanced Raman spectroscopy for the elucidation of complex electrochemical reactions

Alice Fiocco[1,2], Aja A. Pavlic[1], Frédéric Kanoufi[2], Emmanuel Maisonhaute[1], Jean-Marc Noël[2*], Ivan T. Lucas[1,3*]

1 Sorbonne Université, CNRS, Laboratoire Interfaces et Systèmes Electrochimiques, LISE, F-75005 Paris, France

2 Université Paris Cité, CNRS, ITODYS, F-75013 Paris, France

3 Nantes Université, CNRS, IMN, F-44322 Nantes, France

* ivan.lucas@cnrs-imn.fr / jean-marc.noel@cnrs.fr

ABSTRACT: TERS is an emerging nanospectroscopy technique whose implementation *in situ/operando*, namely in liquid phase and under electrochemical polarization (EC-TERS), remains challenging. Investigation of electrochemical processes at the nanoscale, in real time and over wide potential windows can be of particularly interest but tedious when using EC-STM-TERS. This approach was successfully applied to the investigation of a well-established but yet complex system (a thiolated nitrobenzene derivative 4-NBM) whose reduction mechanism involves various multi-steps reaction paths, most likely pH-dependent. In light of the EC-TERS analysis carried out under specific conditions limiting the full (6 e^-/6 H^+) electrochemical reduction of 4-NBM and its photo-coupling, a bimolecular electrochemical reaction path, difficult to evidence from the electrochemical response only, is proposed.

Developing nanoscale-sensitive analytical techniques, which can operate *in situ* or *operando* without the need for ultra-high vacuum, is the prerequisite to the elaboration of new functional (nano)materials and to the understanding of complex processes occurring at their interfaces. Compositional and structural analysis of low cross-section functional materials, *e.g.* 2D, 1D materials and molecular films, can be achieved *via* only a handful of microscopic and spectroscopic techniques. Tip-Enhanced Raman Spectroscopy (TERS, or nanoRaman), which combines Scanning Probe Microscopies (SPMs), Raman microscopy and signal enhancement techniques (SERS) can potentially address this technological gap, although its declination under in situ/operando conditions is still at its early development stage. After its demonstration in the ambient in 2000[1], TERS characterizations at the nanoscale and molecular level were subsequently developed in liquid starting from 2009[2-9], and since 2015 under electrochemical conditions (EC)[10], through the parallel development of top/bottom/side optical coupling of the Raman laser with the TERS-active probe apex (Atomic Force Microscopy probe AFM or Scanning Tunneling Microscopy probe: STM).

The potential-dependent response of 4′-(4-Pyryl)biphenyl-4-methanethiol (4-PBT) molecules[10], the spatially dependent redox behavior of sparse Nile Blue (NB) molecules[11-13], the irreversible reduction of anthraquinone molecules[14], the reactivity mapping of nanoscale defect chemistry on gold surfaces[15], iron and cobalt phthalocyanine deactivation during oxygen reduction reaction[16, 17], and also the reversible transformation (oxidation) of a polyaniline on gold[18] are successful examples of EC-TERS implementation[19-21]. Such redox-active systems were selected based either on i) their strong Raman scattering cross-section at selected excitations (Raman-resonant compounds, at plasmonic junctions), ii) their simple/unequivocal redox reaction scheme (one step, mostly reversible) and/or on their well-established Raman signatures. For more complex electroactive systems involved in multi-steps reactions (electrochemical/chemical) such as those often implicated in electrocatalytic processes, the mechanism of operation can be difficult to decipher. The development of real-time analyses can be particularly relevant for intricate operating processes given that the interfacial composition may evolve under polarization, *i.e.* even using constant potential control).

This EC-TERS study combines *in situ* high-resolution composition mapping under potential control and fast tracking of interfacial TERS signatures upon potential sweeping, with the aim of gaining new insights in the electrochemical transformation of a well-established but yet complex electroactive molecular system involving non-Raman resonant nitrobenzene moieties. Self-assembled monolayers of the thiolated version 4-NTP[22-24], or layers obtained from reduction of nitro-based diazonium precursors[25-28], because of their strong interest for electrode functionalization (sensor[29], molecular electronics[26]), have been the object of thorough electrochemical studies, often combined with spectroscopic-based analyses[30-34], as for such systems, electrochemical tools alone can only give partial information on the mechanism at play.

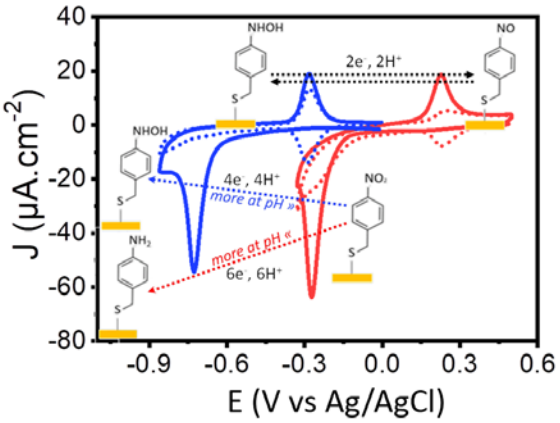

Figure 1. Cyclic voltammetry response of a 4-NBM functionalized gold disk electrode in alkaline medium (pH = 10.7) and in acidic medium (pH = 2.7). The potential was swept respectively between -100 and -850 mV and +500 and -400 mV vs Ag/AgCl, at 50 mV.s^{-1}. The solid and the dotted line represent the first and the second cycle respectively. The chemical transformations of the nitrobenzene moieties and its intermediates are shown in correspondence of the electrochemical peaks.

The complex pH-dependent reduction mechanism, which involves several reaction paths (reversible, irreversible) and intermediates but only one main reduction current peak (see Figure 1) is not fully understood[35, 36]:

- The classically acknowledged reduction path described in Figure 1 & 2 involves three $2e^-/2H^+$ reduction processes, corresponding to the irreversible reduction of the nitro into a nitroso compound, the reversible formation of a hydroxylamine intermediate and its irreversible reduction into an amino moiety.
- A second reaction path (highlighted in blue in Figure 2), involving the chemical reaction of hydroxylamine and nitroso intermediates to form an azoxybenzene dimer (DMAOB), has been proposed in alkaline or neutral media for both "solution" and adsorbed nitrobenzene (thiolated derivative). Under reducing conditions, DMAOB is subjected to another series of $2\ e^-/2\ H^+$ reductions that lead to the formation of azobenzene (*cis*-DMAB for thiolated derivatives), then hydrazobenzene (DMHAB, *via* protonation of the N=N bond), and finally to the cleavage into two 4-ABM moieties.
- Besides, both 4-NTP and its reduced amine form (4-ATP) are subjected to photo-induced coupling, depending on the excitation wavelength, the underlying substrate, or also the surrounding environment[23, 36, 37].

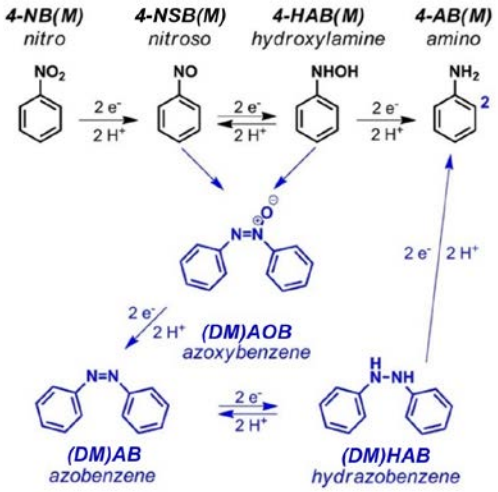

Figure 2. First-order/monomolecular (black) and second-order/bimolecular reaction path (blue) involving the nitrobenzene derivatives. (*DM*) or *(M)* standing for "(di)mercapto" are in brackets, since these mechanisms have been hypothesized for nitrobenzene derivatives either in solution[35] or on surfaces with thiolated derivatives[36]. *Cis* and *trans* isomers are reported for dimers.

In our research group, 4-NTP electrochemical transformation has been previously studied on a tapered gold tip conventionally designed for TERS studies but partially insulated and modified with 4-NTP, thus providing an original single hot-spot EC-SERS platform, the so-called EC-Tip SERS[3]. If the fast irreversible conversion of hydroxylamine/nitroso to 4-ATP has been evidenced in acidic medium at moderate reducing potentials, no reaction intermediates nor dimers could though be detected in the SER spectra.

In work presented hereafter, we have developed a real time EC-STM-TERS configuration to explore *in situ* the reduction mechanism of NB derivatives in alkaline media. Under such conditions where protons are scarce, the lifetime of possible reaction intermediates could be higher, possibly opening alternative reaction path. To this end, an analogue of 4-NTP (non-Raman-resonant) which has a similar electrochemical signature but is less prone to desorption was selected (4-nitrobenzyl mercaptan: 4-NBM).

The spectro-electrochemical analyses were carried out through a thick layer of electrolyte (3mm) using a top-illumination STM-TERS configuration proposed already by our group in 2019,[20] but furtherly developed here to achieve dynamic/real-time signal acquisition (see depiction in Figure 3). Additionally, an original electrochemical polarization strategy, elaborated to circumvent the difficult implementation of EC-STM-TERS on large potential windows[4, 5] was developed.

Experimental section

Reagents and Solutions - 4-nitrobenzyl mercaptan (4-NBM), 4-amino thiophenol (4-ATP), hydroxylamine and azobenzene were purchased from Sigma-Aldrich, nitrosobenzene from TCI. All the compounds were used without further purification. Absolute ethanol, hydrochloric acid (37%) and $NaHCO_3$ (NORMAPUR®) were acquired from VWR, NaOH (analytic grade) and H_2SO_4 (96%) from Carlo Erba Reagents. Gold wires (250 µm diameter) were purchased from MaTecK, Zapon varnish from Laverdure.

Electrochemical activity of functionalized gold electrodes - Self-assembled monolayers (SAM) of 4-NBM were prepared on various gold surfaces (crystalline Au disk electrode / sputtered Au film on mica) and by overnight incubation in 10^{-4} $mol.L^{-1}$ solutions of 4-NBM in absolute ethanol and subsequently rinsed with absolute ethanol (30 minutes). The electrochemical activity of 4-NBM functionalized electrodes was inspected in a pH 10.7 alkaline buffer (mixing of 0.05 $mol.L^{-1}$ $NaHCO_3$ and 0.1 $mol.L^{-1}$ NaOH), as well as in a pH 2.7 H_2SO_4 solution (0.001 $mol.L^{-1}$), in both cases after electrolyte deoxygenation *via* Ar bubbling. Electrochemical measurements were carried out using a 600E potentiostat (CHI) connected to a three-electrode cell (platinum ring counter electrode and an Ag/AgCl reference electrode). The pH 10.7 and 2.7 were chosen as mild conditions to preserve the immersion objective lens used for *in situ* TERS measurements.

EC-TERS measurements - TERS was implemented on a Labram Evolution microspectrophotometer (Horiba Scientific) equipped with an EM-CCD photodetector (Newton 971, Andor Oxford Instruments) and coupled optically to a Scanning Probe Microscope (SPM, OmegaScope, Horiba Scientific/AIST-NT). TERS-active microelectrodes (gold tapered tips) were obtained by electrochemical dissolution of 250 µm diameter gold wires in a HCl/EtOH solution (see description elsewhere[3, 38]) and their partial insulation with a non-Raman-active polymer[20, 38] (Zapon varnish as proposed by Domke's group[4]). The home-made setup enabling electrochemical STM-TERS measurements *via* a top illumination has been described elsewhere[20]. Briefly, a 632.8 nm linearly polarized laser is precisely focused on the apex of the gold tip (at the "hot-spot") using a vertical 40X water-dipping objective (Olympus, LUM PlanFLN, N.A. = 0.8) mounted on a piezo scanner. The partially insulated gold STM tip is slightly bent to reach the focal point of the objective lens (3.3 mm working distance). The control of the electrochemical potential of the TERS-STM probe E_{tip} (working electrode 1 *WE1*) and of the SAM-functionalized gold surface E_{sample} (*WE2*) electrode, and therefore of the STM bias voltage (BV = E_{tip} - E_{sample}), is ensured by a home-made bi-potentiostat[20] connected to a 4-electrode cell (integrated platinum ring counter electrode, while a small size Ag/AgCl reference electrode (3M NaCl, *RE-1B*, Biologic) was approached from the side of the cell).

Electrochemical polarization on large potential window - To explore wide potential ranges while minimizing faradaic reactions at the TERS tips, *WE2* was polarized within the [-100; -850 mV] potential range in the alkaline buffer, and [+150, -600

mV] in the pH 2.7 solution, while maintaining the STM-TERS probe potential fixed at 0 V and +250 mV respectively (BV variation from 0.1 to 0.85 V in both cases). This ensured a net flow of the tunneling current (i_T= 1000 pA) for the dynamic control of the tip-sample distance over time, prerequisite to TERS analyses.

Dynamic EC-TERS acquisition - By synchronizing the EM-CCD photodetector with an arbitrary waveform generator connected to the bi-potentiostat, dynamic STM-TERS measurements (point spectra) were obtained at short acquisition time (down to 0.6 s) and minimal laser power (down to 1% of the nominal laser power ~ 0.16 mW), while scanning the potential at moderately fast rate (cyclic voltammetry CV at 50 mV.s^{-1}). To mitigate possible photothermal degradation/transformation of the SAM at the tip/sample junction upon illumination, the TERS-STM probe was constantly raster scanned during the polarization sequence. The whole setup is depicted in Figure 3, and fully detailed in Figure S1. Time-resolved TERS maps were corrected by the intensity of the background following Ren and coworkers' methodology[39] to correct for wavelength (plasmonic spectral shaping effect: PSSE) and potential effects on the relative intensity of the TERS bands.

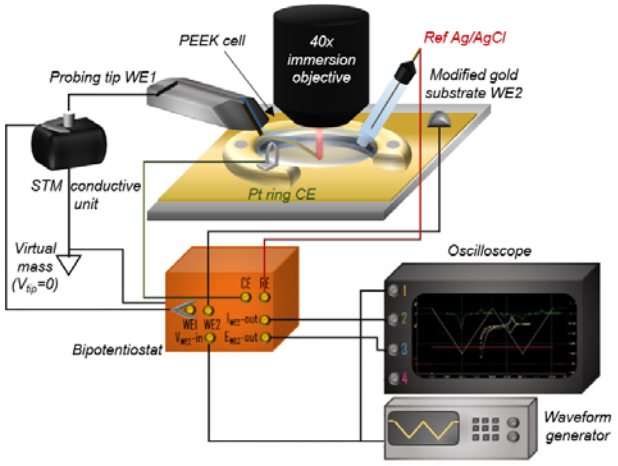

Figure 3. EC-STM-TERS setup developed for nanoscale chemical imaging and real-time tracking of electrochemical reactions on wide potential windows (full description in SI).

Reference spectra - Raman spectra of the analogues of the different compounds and reaction intermediates were collected to ease the interpretation of in situ TERS signatures (see Figure S2, and Table S1).

Results and discussion

Electrochemical signature of the 4-nitrobenzene derivative - The electrochemical response of 4-NBM (cyclic voltammetry at 50 mV.s^{-1}) was first evaluated in alkaline medium (blue curve in Figure 1). Starting from the open circuit potential (OCP), a first irreversible reduction current peak at -730 mV arises during the forward scan of the first cycle, and then reversible (oxidation) current peak in the backward scan at -285 mV. This reversible reduction peak is also observed during the second and following cycles, though weaker in intensity. Similar to the results in the alkaline medium, the CV in acidic medium (pH = 2.7) shows a main reduction peak at -280 mV and the reversible oxidation/reduction peak at higher potential centered on +230 mV, as can be seen on the red curve in Figure 1.

This electrochemical behavior of 4-NBM is consistent with the one of its analogue 4-NTP or other nitrobenzene derivatives widely reported in the literature[35, 38, 40, 41]. The main cathodic peak at more negative potentials is usually ascribed to both the full and irreversible reduction (6 e$^-$/6 H$^+$) of the nitro group into amino (here 4-NBM and 4-ABM respectively) and to the partial reduction into the hydroxylamine intermediate (4-HABM) as seen in Figure 1 (red and blue dotted arrows). The latter can be subsequently reversibly oxidized into the nitroso derivative (4-NSBM) through a reversible 2 e$^-$/2 H$^+$ process associated to the reversible current peak at higher potential. The similarity of the reduction mechanism in the two media is supported by the potential shift of the current peaks (close to that expected for a difference of 8 pH units given a similar e$^-$/H$^+$ ratio) and by the similar intensity of the current peaks. However, the irreversible reduction toward 4-ABM seems less favored in alkaline medium (lower concentration of protons), as suggested by the lower charge ratio between the cathodic and the anodic peaks of the first cycle (1:1 vs 3:1 in acidic conditions) and the slower decrease in intensity of the reversible current peak.

Note that for nitrobenzene moieties in solution (not for adsorbates), an extra reversible peak around [-0.64, -0.69 V] vs SCE has been reported by Gao et al in alkaline medium (pH 13) during the second cycle[35]. This peak which was ascribed to the reversible conversion of DMAB to DMHAB, is not observed here for the thiolated NB derivative.

EC-STM-TERS mapping – After immersion in alkaline electrolyte, the STM-TERS tip (*WE1*) and the SAM-derivatized gold sample (*WE2*) were polarized respectively at E_{tip} = 0 V and at E_{sample} = -100 mV *vs* Ag/AgCl (BV = 0.1 V) for both the tip-sample approach and subsequent hot-spot screening. At such potential values, no electrochemical reaction initially occurs (see first CV on Figure 1). A first STM-TERS map (200 x 100 nm², 50 x 25 pixels, 0.5 s acquisition per pixel) was acquired at E_{sample} = -100 mV. Therefore, a cyclic potential ramp exploring reducing potential ([-100; -850] mV at 50 mV.s^{-1} scan rate) was applied to form 4-HABM *via* the partial reduction of the SAM during the potential ramp. Note that the tip was set off-contact during the CV. Then, while maintaining the probe at E_{tip} = 0 V, two TERS maps were successively acquired at E_{sample} = -100 mV (BV = 0.1 V), where 4-HABM should be oxidized into 4-NSBM, and at E_{sample} = -400 mV (BV = 0.4 V), to reversibly reduce 4-NSBM back to 4-HABM.

Surface topography by EC-STM (200 x 100 nm²), corresponding TERS intensity maps with 4 nm pixel size ("sum" and "overlay": see description below) and spectral signatures averaged on the 50x25 pixels maps as a function of the applied potential are displayed in Figure 1a, b-c and d, respectively. TERS color maps were constructed by summing and comparing the signal intensity of three spectral regions ([blue: 1310-1370], [green: 1420-1480] and [red: 1560-1620] cm^{-1}) that gather the most striking potential-triggered alterations. Despite the non-ideal imaging conditions (bent and ductile polarized STM probe in liquid) and short signal acquisition time (0.5 s), STM and TERS map show matching topography features and TERS intensity fluctuation.

The impact of the electrochemical polarization on the surface composition of the electrode is discussed hereafter:

■ *-100 mV (close to OCP) before reduction* - The average spectrum acquired at the OCP (Figure 4d, top) shows the typical Raman signature of nitrobenzene derivatives, i.e. symmetric NO_2 stretching at 1346 cm^{-1}, ring stretching and the CH bending at 1594 and 1107 cm^{-1} respectively[35, 36]. The presence of a surface feature (interpreted here as a depression) spreading on about 7 pixels (identified by a blue circle on the top map in Figure 1a), correlates with a strong TERS intensity variation (higher number of adsorbed molecule inside the depression

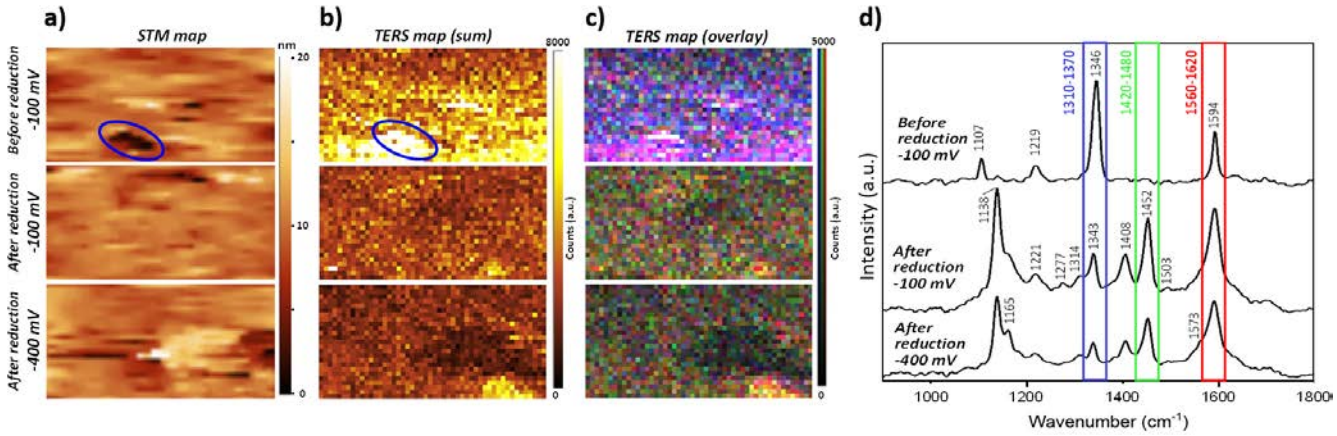

Figure 4. EC-TERS under potential control – a) STM maps, **b)** & **c)** corresponding TERS maps (200 x 100 nm², 50 x 25 pixels²) acquired on a 4-NBM SAM on gold before and after the reduction potential ramp in alkaline medium (pH 10.7), and **d)** spectra averaged on the 50 x 25 pixels² TERS map. TERS color maps (b) and (c) were constructed by summing or comparing the intensity of the three spectral ranges highlighted in blue, red, green and red in (d). The STM-TERS map were achieved at -100 mV *vs* Ag/AgCl (top and middle) before and after a potential ramp exploring reductive potentials or -400 mV (bottom). The tip was temporary retracted during the ramp application. TERS acquisition parameters: t_{acq} = 0.5 s (λ_{exc}: 632.8 nm, power: 250 µW laser power, i.e. 1.5 % of the nominal laser power), tunneling current i_T = 1000 pA, bias voltage BV = 0.1 V (top and middle) or 0.4 V (bottom). The area encircled in blue shows a depression on the gold substrate.

or/and higher enhancement on its edges[42]), yielding an effective lateral resolution of 8-12 nm (see corresponding cross-sectional TERS analysis in Figure S3). Despite intensity fluctuations at surface heterogeneities, the net prevailing of blue/red pixels associated to the NO_2 and ring stretching (Figure 4c, top) suggests a complete surface coverage by molecules still in their nitro state at the OCP.

■ *-100 mV after reduction* - After the reduction ramp, the nitro band is of much smaller intensity, while the intensity of the ring stretching band around 1600 cm^{-1} is conserved (slight increase), implying that no desorption of SAM occurs (or only to a limited extent) and that a large fraction of the surface 4-NBM moieties has been reduced across the screened surface. The broadening of the ring stretching band around 1600 cm^{-1} suggests the presence of new species on the sample surface[35, 36, 43, 44]. The blue shift of the ring stretching band together with the weak signal at 1277 cm^{-1} could traduce the formation of 4-NSBM (NO stretching of nitrosobenzene), expected at -100 mV by oxidation of 4-HABM but also of DMAOB species (see after)[35]. The presence of the two bands at 1452 cm^{-1} and 1408 cm^{-1}, typical of the N=N stretching, along with a lower-energy feature at 1138 cm^{-1}, possibly assigned to C-N stretching[35, 44], indeed suggests the formation of azo compounds (dimer). The dominant green tone in the middle color map of Figure 4c (green color corresponding to the 1420-1480 cm^{-1} energy range) suggests that dimers are the prevailing reaction products upon reduction of 4-NBM.

■ *-400 mV after reduction* - Interestingly, the overall spectral profile does not change significantly when lowering the sample potential down to -400 mV, the absence of the weak intensity band at 1277 cm^{-1} being the only feature supporting the conversion of 4-NSBM to 4-HABM. The azobenzene signatures keep being dominant (as suggested by the bottom TERS map in Figure 4c), while no other spectral features clearly appear.

Dynamic observation of 4-NBM SAM reduction process on large potential windows - To get a clearer picture of the dynamic of disappearance/appearance of spectral features as a function of the electrochemical polarization, real-time monitoring of the nitrobenzene derivative reduction was then achieved upon potential scan. The potential, current and spectral evolutions with time are shown in Figure 5a-b.

A specific sample electrochemical polarization sequence was designed to maximize the possible TERS detection of possible intermediates around the reversible current peak after a brief exploration of reductive potentials: (1) initial polarization at E_{sample} = -100 mV (~ OCP) for 5 s; (2) a first potential ramp down to -850 mV ("forward" scan at 50 $mV.s^{-1}$); (3) a second potential ramp up to -390 mV (backward scan); (4) a constant polarization at -390 mV (20 s); (5) a third ramp up to -100 mV; (6) a constant polarization at -100 mV for 5 s. Note that E_{tip} was maintained constant at 0 V during the whole potential exploration to minimize stray electrochemical reduction current at the tip, implying that bias voltage spanned between 0.1 V and 0.85 V. TERS spectra averaged over the time periods associated to 6 polarization steps (gray dots of Figure 5a) are also given in Figure 5c. The whole set of spectral data is given in Figure S5.

Tracking of the TERS signal turned out successful on the whole potential range explored despite the large BV values used (around 0.85 V in the lowest potential limit of the voltammogram). The large variation of STM BV upon potential exploration is indeed expected to result in some intensity loss directly related to the variation of the tip−sample distance and of the local field enhancement[4], with however a lesser impact in aqueous medium as compared to the air[5]. A ~ 2.5 TERS intensity damping (on background corrected data) for the ring stretching mode around 1600 cm^{-1} is observed here on the [0.1- 0.85V] BV range, the initial intensity is recovered upon decreasing the BV back to 0.1V[5] (see Figure S6).

A multivariate analysis of the potential depend TERS spectra (see SI) allowed to extract on the whole potential range explored only two main compositions, whose signatures match the one of 4-NBM and of the dimer (Figure S7 & S8). The spectral signature of 4-NBM (NO_2 and ring stretching bands) is identified from the OCP down to ~ -300 mV, then decreases in intensity and disappears completely at around -700 mV in correspondence with the cathodic peak (Figure 5a).

Concomitantly, the signature of the dimer (C-H bending / C-N stretching of azobenzene: 1100-1200 cm^{-1}, N=N stretching: 1400-1500 cm^{-1}) progressively appears and become neater after the potential scan direction is reversed from -850 mV up to -

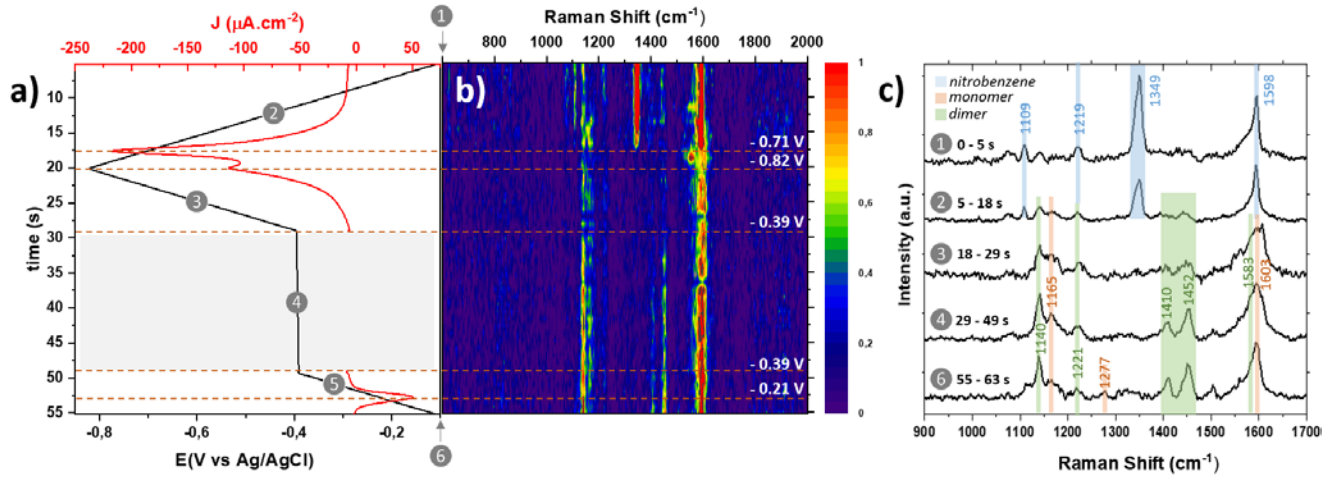

Figure 5. Dynamic TERS measurements – **a)** Time-evolution of potential, current density and **b)** corresponding TERS signatures (background subtracted time map) of a 4-NBM SAM on gold in alkaline medium (pH 10.7), **c)** average spectra corresponding to the 5 electrochemical polarization steps marked as gray dots 1, 2, 3, 4, 5 in (**a**). Potential ramps (2) [-100; -850 mV], (3) [-850; -390 mV], (4) [-390; -100 mV] were carried out at 50 mV.s^{-1}, chronoamperometric steps (1), (4), (6) at -100 mV (5s), -390 (20s) and -100 mV (5s) respectively. TERS acquisition parameters: t_{acq} = 1 s, λ_{exc} = 632.8 nm laser line, power: 160 µW laser power (i.e. 1 % of the nominal laser power), tunneling current i_T = 1000 pA, bias voltage BV: 0.1 to 0.85 V. The full set of spectra can be found in Figure S5.

400 mV and maintained constant (polarization step at -400 mV). I_{TERS} vs E(V) plots depicted in Figure 6 and S9 confirm this trend, showing clear azo bond bands at 1452 cm^{-1} at high negative polarization only (-650/-700 mV) when the nitro band is about to disappear and continuous intensity increase during the backward scan. Note that no strong spectral changes are observed upon scanning the potential across the range associated to the anodic peak (see EC response in Figure 5a-b), usually ascribed to the conversion of hydroxylamine 4-HABM into nitroso 4-NSBM. The emergence of a weak signal at 1277 cm^{-1} is the only noticeable change possibly attributed to the NO stretching of 4-NSBM (or DMAOB species) as mentioned earlier (see spectrum 3 in Figure 5c). The dynamic TERS evaluation confirms dimers as one of the prevalent reaction products in the studied conditions and suggests that the electrochemical polarization triggers dimerization, concomitantly to the 4e$^-$ sequential reduction process 4-NBM → 4-NSBM → 4-HABM.

Discussion on the reduction mechanism - Although some of the bands enlightened in green in Figure 5c were assigned to the C-N stretching and the N=N modes of azobenzene moieties, the unequivocal identification of their origin requires a deeper analysis as dimers can be formed either through a photo-activated path (light-induced dimerization) or through a "bimolecular" electrochemical path. Note that such bands had been also attributed to the amino derivative during EC-SERS experiments in alkaline medium [45], this assignment was however later-on dismissed by Huang *et al*[48, 49] and won't be therefore considered here.

■ *Photo vs potential-induced dimerization* - Photochemical coupling has been reported for both nitro[46] and amino[47-49] benzene derivatives, through the combined effects of surface plasmon resonance (SPR) on capped Ag or Au nanostructures, illuminated with green (514.5 nm) and red laser sources (632.8 nm) usually under high photon flux (up to 650 µW to detect a 1:1 intensity ratio between 4-ATP and DMAB bands), mostly in the ambient but also in liquid and polarization[48, 49]. Observation of *trans* but also *cis* DMAB isomers has been also reported by El Khoury[8] by TERS analysis of 4-NTP on gold in water. Moreover, Koopman *et al*.[50] underlined that the flexibility of 4-NBM molecules, provided by the methyl between the sulfur and the benzene ring, favors the formation of dimeric species upon illumination.

The influence of the irradiation on the TERS response of 4-NBM at the tip-sample junction was therefore evaluated *in situ* in the alkaline buffer at the OCP, using the 632.8 nm laser line at increasing laser power. No "dimeric" bands can be detected for 4-NBM even at the highest power 4 mW (which only induces an increase in the background signal, as can be seen in Figure S10), ruling out possible photo-dimerization effects. As for 4-ATP, the azo bands only started appearing at laser powers as high as 1.6 mW, thus 10 times higher than in the abovementioned TERS conditions (see Figure S11). Therefore, the use of a 632.8 nm excitation source (at low laser power 160 µW), the implementation in a liquid environment with reduced oxygen content and the constant raster scanning of the TERS tip over the surface should cancel out possible chemical transformations induced by photocatalytic processes during the EC-TERS experiments.

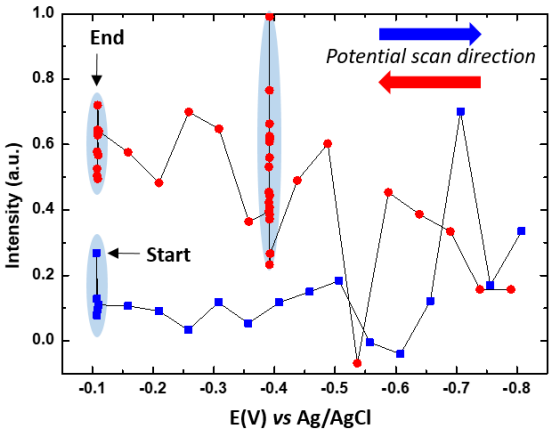

Figure 6. TERS-CV - Variation in alkaline medium of the 1452 cm^{-1} band intensity with the potential applied to the sample through continuous modification of the STM bias voltage. The intensity was corrected, considering the variation of the TERS signal enhancement upon BV sweeping. The data points enlightened in clear blue correspond to the polarization steps at constant potential (see full description in SI).

The fact that the 1452 cm^{-1} dimer band intensity remains at the noise level upon potential sweeping from the OCP down to -650mV as shown on Figure 6, supports this claim. Moreover, the striking synchronicity between the disappearance of the nitro band and the appearance of the azo bond bands at 1452 cm^{-1} suggests a dimer formation triggered by the electrochemical polarization, although a combined/synergetic polarization and illumination effects cannot be fully excluded.

■ *Influence of the pH* – As the lack of proton availability is incriminated here as a possible origin of the limited reduction process and the promotion of dimer formation, the effect of pH was evaluated below. 4-NBM SAM on gold was first subjected to electrochemical reduction conditions in alkaline medium at pH 10.7 (same polarization sequence as described earlier) then to electrochemical reduction in acid medium at pH 2.7 (the electrolyte filling the 4-electrode cell was changed to a 1 $mmol.L^{-1}$ H_2SO_4 solution). Note that the potential range in acidic medium was readjusted to +150/-600 mV *vs* Ag/AgCl. After transfer to acidic medium, the cathodic peak at lower potential on the second CV of Figure 7a (red curve) is still of high intensity (see for comparison the 2nd CV that should have been obtained at pH 10.7 in Figure 1), and the anodic peak associated to the 4-HABM-to-4-NSBM reversible conversion is absent. These observations suggest that only a fraction of 4-NBM was initially reduced in an irreversible manner during the first CV cycle in alkaline medium (e.g. into 4-ABM or DMAB) and therefore that some monomolecular intermediates were still available for reduction during the following cycle in acidic medium.

However, the persistence of the TERS bands located in the green energy ranges in Figure 7b (spectrum 4) after transfer of reduced 4-NBM to acidic medium, suggest that DMAB-type dimers (possibly also DMAOB or DMHAB) are one of the main reduction products obtained upon reduction of a 4-NBM SAM in the employed experimental conditions. The slow conversion of hydroxylamine into amine and the stronger electrophilicity of the nitroso group[36] could explain the promotion of such dimer formation in neutral and alkaline conditions.

The persistence of the bands attributed to the dimers still after and even after a second potential ramp, where full reduction of DMAB dimers (possibly also DMAOB or DMHAB) to amino could be expected following Gao's mechanism, seems to attest of the high stability of the dimeric species under the employed conditions. The electrochemical steps corresponding to reduction of DMAB to DMHAB and 4-ABM as described in Figure 2 then do not seems to occur under the present conditions (4-NBM precursor, lack of proton availability).

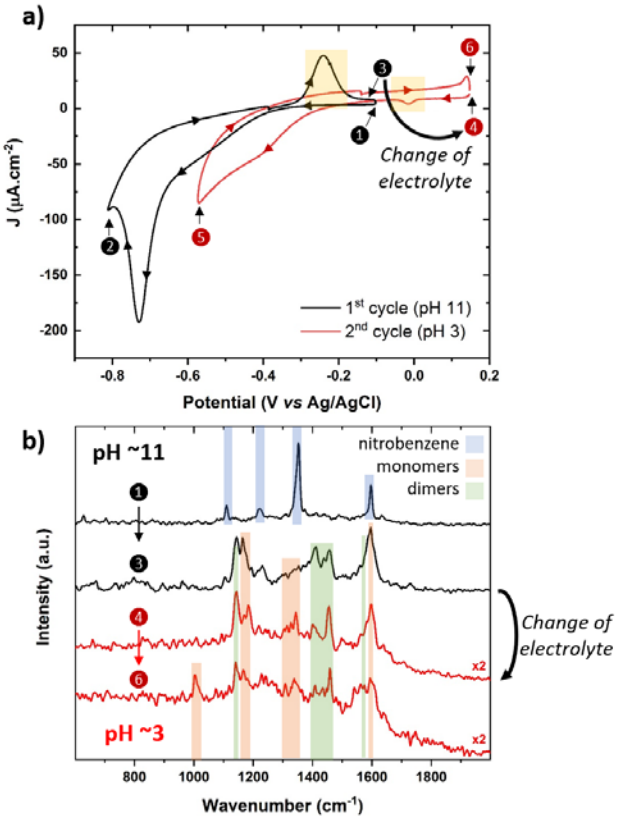

Figure 7. pH effect - a) Reconstructed CV curves from a 4-NBM SAM on gold in alkaline medium (black curve: 1st cycle in a bicarbonate buffer at pH 10.7, [-100, -800 mV], scan rate 50 $mV.s^{-1}$) and after transfer to acidic medium (red curve: 2nd cycle in H_2SO_4 at pH 2.7, [+150 and - 600 mV]); **b)** corresponding TER spectra. Each spectrum in (a) is the average of the five spectra acquired during the first or the last chronoamperometric step (i.e. step (I) or (VI)). TERS parameters: t_{acq} = 1 s, λ_{exc} = 632.8 nm, power = 160 µW (i.e. 1 % of the nominal laser power), tunneling current i_T = 1000 pA, variable bias voltage BV between 0.1 V and 0.8 V. The intensities of the spectra in acid medium were multiplied by a factor 2. Numbers 1-6 are given to ease the reading of the electrochemical sequence.

■ *Dimer stability* - Note that a reversible conversion of DMAB to DMHAB (reversible current peak at - 0.64 V vs SCE) had been reported by Gao *et al.*[35] for both nitrobenzene and nitrosobenzene in solution only (not for adsorbates) and in alkaline medium only (pH 13), whereas the full and irreversible reduction of adsorbed DMAB into 4-ATP onto roughened Ag has been evidenced by Huang *et al.*[48, 49] in neutral medium ($NaClO_4$) and at potential more negative than 0.8V. The absence of additional electrochemical features in alkaline medium as compared to acidic medium as shown in Figure 1, together with the absence of 4-ABM signature further support our claim that thiolated dimers once formed are stable and do not undergo further reduction. The stability of the 4-NBM-derived dimers has been already pointed out by Koopman *et al.*[50], although under different experimental conditions. The promotion of dimers formation upon illumination due to the higher flexibility of 4-NBM molecules as compared to 4-NTP, as suggested in the same study, may also apply under electrochemical conditions. The observation of DMAB-like spectral signatures by TERS in alkaline medium in spite of the absence of characteristic features on the electrochemical response of the functionalized electrode is not surprising, as the main reduction current peak,

quite broad, hosts both the nitro partial and total reduction processes and as protons may be too scarce at the electrode/electrolyte interface for the reversible opening of the azo compound (DMAB into DMHAB) to take place in the experimental conditions used here.

Conclusions

In this work, real-time STM-TERS measurements were implemented to investigate *in situ* the electrochemical transformation of 4-NBM, an analogue of the largely studied 4-NTP nitrobenzene derivative, self-assembled on gold electrodes. Alkaline medium was considered in order to slow down the reduction rate of the nitrobenzene reduction reaction (at low proton content), possibly promoting an alternative bimolecular reaction path. The formation of DMAB dimers under 4-NBM reduction, was evidenced by STM-TERS imaging at fixed potential, and confirmed by dynamic STM-TERS measurements, successfully implemented at moderate potential scan rate (50 $mV.s^{-1}$) and on large potential windows (up to 850 mV). Particularly, the electrochemical formation of DMAB was evidenced under experimental conditions where the photo-assisted formation of dimers could be neglected. This study demonstrates the robustness and pertinence of *in situ*/*operando* TERS analyses applied to redox-active molecular compounds at a plasmonic junction (metal tip-molecule-metal substrate junction). It opens new routes for the characterization of more complex systems (such as redox-active inorganic/organic films with multiple redox centers, catalytic nanomaterial on metallic or dielectric substrates).

ASSOCIATED CONTENT

Supporting Information

Extra material can be found as supporting information: a detail description of the EC-TERS set-up, the µRaman spectra of compounds and reaction intermediates mentioned in the study (powder), the vibration modes assignment of the benzene derivative Raman spectra; the analysis of the EC-TERS spatial and time maps, the spectra of 4-NBM and 4-ATP SAM subjected to increasing laser power. The Supporting Information is available free of charge on the ACS Publications website.

AUTHOR INFORMATION

Corresponding Author

* (I.T.L.) E-mail: ivan.lucas@cnrs-imn.fr / ivan.lucas@sorbonne-universite.fr
***** **(**J.-M**.**N) E-mail: jean-marc.noel@u-paris.fr
ORCID
Ivan T. Lucas: 0000-0001-8930-0437
Jean-Marc Noël: 0000-0001-8278-7748
Frédéric Kanoufi: 0000-0002-9784-2380
Emmanuel Maisonhaute: 0000-0001-6337-7436

Author Contributions

I.T.L., E.M., J.-M.N., F.K., A.F. designed the experiments. A.F. collected all the data. A.A.P. collected AFM-TERS and electrochemical data (not presented here) on the same system which confirmed the STM-TERS data shown in this work. I.T.L., E.M., J.-M.N., F.K. & A.F. contributed to the elaboration of the manuscript.

ACKNOWLEDGMENT

Acknowledgments go to the LabEx Michem (n°ANR: 10-LABX-0068) of Sorbonne Université (Paris, France) for their financial support.

REFERENCES

(1) Stöckle, R. M.; Suh, Y. D.; Deckert, V.; Zenobi, R. Nanoscale chemical analysis by tip-enhanced Raman spectroscopy. *Chem. Phys. Lett.* **2000**, *318* (1-3), 131-136.
(2) Schmid, T.; Yeo, B.-S.; Leong, G.; Stadler, J.; Zenobi, R. Performing tip-enhanced Raman spectroscopy in liquids. *J. Raman Spectrosc.* **2009**, *40* (10), 1392-1399.
(3) Touzalin, T.; Dauphin, A. L.; Joiret, S.; Lucas, I. T.; Maisonhaute, E. Tip enhanced Raman spectroscopy imaging of opaque samples in organic liquid. *Phys. Chem. Chem. Phys.* **2016**, *18* (23), 15510-15513.
(4) Martin Sabanes, N.; Driessen, L. M.; Domke, K. F. Versatile Side-Illumination Geometry for Tip-Enhanced Raman Spectroscopy at Solid/Liquid Interfaces. *Anal. Chem.* **2016**, *88* (14), 7108-7114.
(5) Sabanes, N. M.; Elizabeth, A.; Pfisterer, J. H. K.; Domke, K. F. The effect of STM parameters on tip-enhanced Raman spectra. *Faraday Discuss.* **2017**, *205*, 233-243.
(6) Kumar, N.; Su, W.; Vesely, M.; Weckhuysen, B. M.; Pollard, A. J.; Wain, A. J. Nanoscale chemical imaging of solid-liquid interfaces using tip-enhanced Raman spectroscopy. *Nanoscale* **2018**, *10* (4), 1815-1824.
(7) Bhattarai, A.; Joly, A. G.; Krayev, A.; El-Khoury, P. Z. Taking the Plunge: Nanoscale Chemical Imaging of Functionalized Gold Triangles in H2O via TERS. *J. Phys. Chem. C* **2019**, *123* (12), 7376-7380.
(8) Bhattarai, A.; El-Khoury, P. Z. Nanoscale Chemical Reaction Imaging at the Solid-Liquid Interface via TERS. *J. Phys. Chem. Lett.* **2019**, *10* (11), 2817-2822.
(9) El-Khoury, P. Z. Tip-Enhanced Raman Chemical and Chemical Reaction Imaging in H(2)O with Sub-3-nm Spatial Resolution. *J. Am. Chem. Soc.* **2023**, *145* (12), 6639-6642.
(10) Zeng, Z. C.; Huang, S. C.; Wu, D. Y.; Meng, L. Y.; Li, M. H.; Huang, T. X.; Zhong, J. H.; Wang, X.; Yang, Z. L.; Ren, B. Electrochemical Tip-Enhanced Raman Spectroscopy. *J. Am. Chem. Soc.* **2015**, *137* (37), 11928-11931.
(11) Kurouski, D.; Mattei, M.; Van Duyne, R. P. Probing Redox Reactions at the Nanoscale with Electrochemical Tip-Enhanced Raman Spectroscopy. *Nano Lett.* **2015**, *15* (12), 7956-7962.
(12) Kang, G.; Yang, M.; Mattei, M. S.; Schatz, G. C.; Van Duyne, R. P. In Situ Nanoscale Redox Mapping Using Tip-Enhanced Raman Spectroscopy. *Nano Lett.* **2019**, *19* (3), 2106-2113.
(13) Chen, X.; Goubert, G.; Jiang, S.; Van Duyne, R. P. Electrochemical STM Tip-Enhanced Raman Spectroscopy Study of Electron Transfer Reactions of Covalently Tethered Chromophores on Au(111). *J. Phys. Chem. C* **2018**, *122* (21), 11586-11590.
(14) Huang, S. C.; Ye, J. Z.; Shen, X. R.; Zhao, Q. Q.; Zeng, Z. C.; Li, M. H.; Wu, D. Y.; Wang, X.; Ren, B. Electrochemical Tip-Enhanced Raman Spectroscopy with Improved Sensitivity Enabled by a Water Immersion Objective. *Anal. Chem.* **2019**, *91* (17), 11092-11097.
(15) Pfisterer, J. H. K.; Baghernejad, M.; Giuzio, G.; Domke, K. F. Reactivity mapping of nanoscale defect chemistry under electrochemical reaction conditions. *Nat. Commun.* **2019**, *10* (1), 5702.
(16) Chen, Z.; Jiang, S.; Kang, G.; Nguyen, D.; Schatz, G. C.; Van Duyne, R. P. Operando Characterization of Iron Phthalocyanine Deactivation during Oxygen Reduction Reaction Using Electrochemical Tip-Enhanced Raman Spectroscopy. *J. Am. Chem. Soc.* **2019**, *141* (39), 15684-15692.
(17) Jiang, S.; Chen, Z.; Chen, X.; Nguyen, D.; Mattei, M.; Goubert, G.; Van Duyne, R. P. Investigation of Cobalt Phthalocyanine at the Solid/Liquid Interface by Electrochemical Tip-Enhanced Raman Spectroscopy. *J. Phys. Chem. C* **2019**, *123* (15), 9852-9859.
(18) Bao, Y. F.; Cao, M. F.; Wu, S. S.; Huang, T. X.; Zeng, Z. C.; Li, M. H.; Wang, X.; Ren, B. Atomic Force Microscopy Based Top-Illumination Electrochemical Tip-Enhanced Raman Spectroscopy. *Anal. Chem.* **2020**, *92* (18), 12548-12555.
(19) Martín Sabanés, N.; Ohto, T.; Andrienko, D.; Nagata, Y.; Domke, K. F. Electrochemical TERS Elucidates Potential-Induced Molecular Reorientation of Adenine/Au(111). *Angew. Chem.* **2017**, *129* (33), 9928-9933.
(20) Touzalin, T.; Joiret, S.; Lucas, I. T.; Maisonhaute, E. Electrochemical tip-enhanced Raman spectroscopy imaging with 8 nm lateral resolution. *Electrochem. Comm.* **2019**, *108*, 106557.
(21) Huang, S. C.; Bao, Y. F.; Wu, S. S.; Huang, T. X.; Sartin, M. M.; Wang, X.; Ren, B. Electrochemical Tip-Enhanced Raman Spectroscopy:

An In Situ Nanospectroscopy for Electrochemistry. *Annu. Rev. Phys. Chem.* **2021**, *72*, 213-234.
(22) Schwamborn, S.; Stoica, L.; Neugebauer, S.; Reda, T.; Schmidt, H. L.; Schuhmann, W. Local modulation of the redox state of p-nitrothiophenol self-assembled monolayers using the direct mode of scanning electrochemical microscopy. *ChemPhysChem* **2009**, *10* (7), 1066-1070.
(23) Dong, B.; Fang, Y.; Chen, X.; Xu, H.; Sun, M. Substrate-, wavelength-, and time-dependent plasmon-assisted surface catalysis reaction of 4-nitrobenzenethiol dimerizing to p,p'-dimercaptoazobenzene on Au, Ag, and Cu films. *Langmuir* **2011**, *27* (17), 10677-10682.
(24) van Schrojenstein Lantman, E. M.; Deckert-Gaudig, T.; Mank, A. J.; Deckert, V.; Weckhuysen, B. M. Catalytic processes monitored at the nanoscale with tip-enhanced Raman spectroscopy. *Nat. Nanotechnol.* **2012**, *7* (9), 583-586.
(25) Laurentius, L.; Stoyanov, S. R.; Gusarov, S.; Kovalenko, A.; Du, R.; Lopinski, G. P.; McDermott, M. T. Diazonium-derived aryl films on gold nanoparticles: evidence for a carbon-gold covalent bond. *ACS Nano* **2011**, *5* (5), 4219-4227.
(26) Fan, X. Y.; Nouchi, R.; Yin, L. C.; Tanigaki, K. Effects of electron-transfer chemical modification on the electrical characteristics of graphene. *Nanotechnol.* **2010**, *21* (47), 475208.
(27) Hartig, P.; Rappich, J.; Dittrich, T. Engineering of Si surfaces by electrochemical grafting of p-nitrobenzene molecules. *Appl. Phys. Lett.* **2002**, *80* (1), 67-69.
(28) Richard, W.; Evrard, D.; Busson, B.; Humbert, C.; Dalstein, L.; Tadjeddine, A.; Gros, P. The reduction of 4-nitrobenzene diazonium electrografted layer: An electrochemical study coupled to in situ sum-frequency generation spectroscopy. *Electrochim. Acta* **2018**, *283*, 1640-1648.
(29) Vijaikanth, V.; Capon, J.-F.; Gloaguen, F.; Schollhammer, P.; Talarmin, J. Chemically modified electrode based on an organometallic model of the [FeFe] hydrogenase active center. *Electrochem. Comm.* **2005**, *7* (4), 427-430.
(30) Shindo, H. Raman spectroscopic observation of adsorbates on Ag during electrochemical reduction of nitrobenzene. *J. Chem. Soc., Faraday Trans. 1* **1986**, *82* (1), 45.
(31) Nielsen, J. U.; Esplandiu, M. J.; Kolb, D. M. 4-Nitrothiophenol SAM on Au(111) Investigated by in Situ STM, Electrochemistry, and XPS. *Langmuir* **2001**, *17* (11), 3454-3459.
(32) Médard, C.; Morin, M. Chemisorption of aromatic thiols onto a glassy carbon surface. *J. Electroanal. Chem.* **2009**, *632* (1-2), 120-126.
(33) Lehr, J.; Williamson, B. E.; Flavel, B. S.; Downard, A. J. Reaction of gold substrates with diazonium salts in acidic solution at open-circuit potential. *Langmuir* **2009**, *25* (23), 13503-13509.
(34) Laforgue, A.; Addou, T.; Belanger, D. Characterization of the deposition of organic molecules at the surface of gold by the electrochemical reduction of aryldiazonium cations. *Langmuir* **2005**, *21* (15), 6855-6865.
(35) Gao, P.; Gosztola, D.; Weaver, M. L. Coupling real-time surface-enhanced raman spectroscopy with linear-sweep voltammetry. *Anal. Chim. Acta* **1988**, *212*, 201-212.
(36) Zhao, L.-B.; Chen, J.-L.; Zhang, M.; Wu, D.-Y.; Tian, Z.-Q. Theoretical Study on Electroreduction of p-Nitrothiophenol on Silver and Gold Electrode Surfaces. *J. Phys. Chem. C* **2015**, *119* (9), 4949-4958.
(37) Miao, P.; Ma, Y.; Sun, M.; Li, J.; Xu, P. Tuning the SERS activity and plasmon-driven reduction of p-nitrothiophenol on a Ag@MoS(2) film. *Faraday Discuss.* **2019**, *214* (0), 297-307.
(38) Touzalin, T.; Joiret, S.; Maisonhaute, E.; Lucas, I. T. Complex Electron Transfer Pathway at a Microelectrode Captured by in Situ Nanospectroscopy. *Anal. Chem.* **2017**, *89* (17), 8974-8980.
(39) Lin, K. Q.; Yi, J.; Zhong, J. H.; Hu, S.; Liu, B. J.; Liu, J. Y.; Zong, C.; Lei, Z. C.; Wang, X.; Aizpurua, J.; Esteban, Ren B. Plasmonic photoluminescence for recovering native chemical information from surface-enhanced Raman scattering. *Nat. Commun.* **2017**, *8*, 14891.
(40) Cyr, A.; Huot, P.; Marcoux, J.-F.; Belot, G.; Laviron, E.; Lessard, J. The electrochemical reduction of nitrobenzene and azoxybenzene in neutral and basic aqueous methanolic solutions at polycrystalline copper and nickel electrodes. *Electrochim. Acta* **1989**, *34* (3), 439-445.
(41) López, I.; Cesbron, M.; Levillain, E.; Breton, T. Diazonium Grafting Control through a Redox Cross-Reaction: Elucidation of the Mechanism Involved when using 2,2-Diphenylpicrylhydrazyl as an Inhibitor. *ChemElectroChem* **2018**, *5* (8), 1197-1202.
(42) Merlen, A.; Plathier, J.; Ruediger, A. A near field optical image of a gold surface: a luminescence study. *Phys. Chem. Chem. Phys.* **2015**, *17* (33), 21176-21181.
(43) Madzharova, F.; Heiner, Z.; Guhlke, M.; Kneipp, J. Surface-Enhanced Hyper-Raman Spectra of Adenine, Guanine, Cytosine, Thymine, and Uracil. *J. Phys. Chem. C* **2016**, *120* (28), 15415-15423.
(44) Gruger, A.; Le Calvé, N. Spectres de vibration du trans-azoxybenzène et de quelques dérivés isotopiques. *Spectrochim. Acta A Mol. Spectrosc.* **1972**, *28* (7), 1253-1262.
(45) Kim, K.; Kim, K. L.; Shin, D.; Choi, J.-Y.; Shin, K. S. Surface-Enhanced Raman Scattering of 4-Aminobenzenethiol on Ag and Au: pH Dependence of b2-Type Bands. *J. Phys. Chem. C* **2012**, *116* (7), 4774-4779.
(46) Zhang, Z.; Kinzel, D.; Deckert, V. Photo-Induced or Plasmon-Induced Reaction: Investigation of the Light-Induced Azo-Coupling of Amino Groups. *J. Phys. Chem. C* **2016**, *120* (37), 20978-20983.
(47) Xu, J. F.; Luo, S. Y.; Liu, G. K. Different behaviors in the transformation of PATP adsorbed on Ag or Au nanoparticles investigated by surface-enhanced Raman spectroscopy - a study of the effects from laser energy and annealing. *Spectrochim Acta A Mol Spectrosc.* **2015**, *143*, 35-39.
(48) Huang, Y. F.; Zhu, H. P.; Liu, G. K.; Wu, D. Y.; Ren, B.; Tian, Z. Q. When the signal is not from the original molecule to be detected: chemical transformation of para-aminothiophenol on Ag during the SERS measurement. *J. Am. Chem. Soc.* **2010**, *132* (27), 9244-9246.
(49) Huang, Y.-F.; Wu, D.-Y.; Zhu, H.-P.; Zhao, L.-B.; Liu, G.-K.; Ren, B.; Tian, Z.-Q. Surface-enhanced Raman spectroscopic study of p-aminothiophenol. *Phys. Chem. Chem. Phys.* **2012**, *14* (24), 8485-8497, 10.1039/C2CP40558J.
(50) Koopman, W.; Titov, E.; Sarhan, R. M.; Gaebel, T.; Schürmann, R.; Mostafa, A.; Kogikoski, S.; Milosavljević, A. R.; Stete, F.; Liebig, F.; Schmitt C.N.Z., Koetz J., Bald. I, Saalfrank P., Bargheer M. The Role of Structural Flexibility in Plasmon-Driven Coupling Reactions: Kinetic Limitations in the Dimerization of Nitro-Benzenes. *Adv. Mater. Interfaces* **2021**, *8*, 2101344.

For TOC only